



PCCP

**Extreme Ultraviolet Time-Resolved Photoelectron Spectroscopy of Adenine, Adenosine and Adenosine Monophosphate in a Liquid Flat Jet**

Journal:	<i>Physical Chemistry Chemical Physics</i>
Manuscript ID	CP-ART-02-2024-000856.R1
Article Type:	Paper
Date Submitted by the Author:	06-Apr-2024
Complete List of Authors:	Koga, Masafumi; University of California Berkeley, Chemistry Kang, Do Hyung; University of California Berkeley, Chemistry Heim, Zachary; University of California Berkeley, Chemistry Meyer, Philipp; Ruhr University Bochum, Physical Chemistry 2 Erickson, Blake; University of California Berkeley, Chemistry Haldar, Neal; University of California Berkeley, Chemistry Baradaran, Negar; University of California Berkeley, Chemistry Havenith, Martina; Ruhr Universitat Bochum, Neumark, Daniel; University of California, Dept of Chemistry; Lawrence Berkeley National Laboratory, Chemical Sciences Division

SCHOLARONE™  
Manuscripts

1  
2  
3  
4  
5  
6  
7  
8  
9  
10  
11  
12  
13  
14  
15  
16

# Extreme Ultraviolet Time-Resolved Photoelectron Spectroscopy of Adenine, Adenosine and Adenosine Monophosphate in a Liquid Flat Jet

*Masafumi Koga,<sup>1</sup> Do Hyung Kang,<sup>1</sup> Zachary N. Heim,<sup>1</sup> Philipp Mayer,<sup>2</sup> Blake A. Erickson,<sup>1</sup> Neal Haldar,<sup>1</sup> Negar Baradaran,<sup>1</sup> Martina Havenith<sup>2</sup> and Daniel M. Neumark<sup>1,3\*</sup>*

<sup>1</sup>*Department of Chemistry, University of California, Berkeley, California 94720, USA*

<sup>2</sup>*Lehrstuhl für Physikalische Chemie II, Ruhr-Universität Bochum, 44801, Germany*

<sup>3</sup>*Chemical Sciences Division, Lawrence Berkeley National Laboratory, Berkeley, California 94720, USA*

\* Corresponding author. Email: [dneumark@berkeley.edu](mailto:dneumark@berkeley.edu)

1 **Abstract**

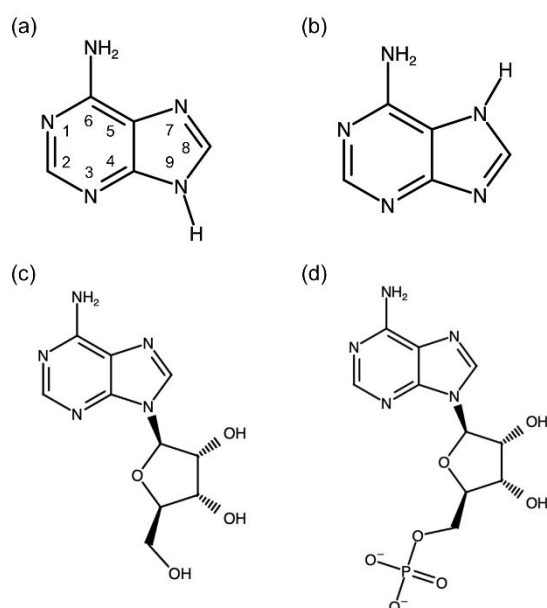
2

3 Time-resolved photoelectron spectroscopy using an extreme-ultraviolet (XUV) probe pulse  
4 was used to investigate the UV photoinduced dynamics of adenine (Ade), adenosine (Ado),  
5 and adenosine-5-monophosphate (AMP) in a liquid water jet. Unlike previous studies using  
6 UV probe pulses, the XUV pulse at 21.7 eV can photoionize all excited states of a molecule,  
7 allowing for full relaxation pathways to be addressed after excitation at 4.66 eV. This work  
8 was carried out using a gas-dynamic flat liquid jet, resulting in a considerably enhanced signal  
9 compared to a cylindrical jet. All three species decay on multiple time scales that are assigned  
10 based on their decay associated spectra; the fastest decay of  $\sim 100$  fs is assigned to  $\pi\pi^*$  decay  
11 to the ground state, while the smaller component with a lifetime of  $\sim 500$  fs is attributed to the  
12  $n\pi^*$  state. An additional slower channel in Ade is assigned to the 7H Ade conformer, as seen  
13 previously. This work demonstrates the capability of XUV-TRPES to disentangle non-  
14 adiabatic dynamics in an aqueous solution in a state-specific manner and represents the first  
15 identification of the  $n\pi^*$  state in the relaxation dynamics of adenine and its derivatives.

16

## 1 1 Introduction

2 The photophysics and photochemistry of nucleic acid constituents (NACs) are of fundamental  
3 interest from the perspective of understanding biological damage induced by ultraviolet light.<sup>1-3</sup>  
4 Despite the large cross sections of NACs in the ultraviolet (UV) regime, DNA is known to be  
5 remarkably photostable, as evidenced by the quantum yields of photodamage being less than  
6 1%.<sup>4, 5</sup> Research has focused on elucidating the underlying mechanisms of photostability, i.e.  
7 how the excess energy is efficiently dissipated in a non-destructive manner before inducing  
8 bond cleavage that can lead to biological damage.<sup>6-11</sup> A better understanding of the processes  
9 at the molecular level is crucial not only for a bottom-up understanding biological effects of  
10 the UV light, but for elucidating the reasons for the selection of nucleobases as the elements of  
11 building blocks that define the genetic code.<sup>12, 13</sup> To this end, we have applied extreme  
12 ultraviolet time-resolved photoelectron spectroscopy (XUV-TRPES) to investigate the  
13 relaxation dynamics of aqueous adenine (Ade), its nucleoside adenosine (Ado), and nucleotide  
14 adenosine-5-monophosphate (AMP), the structures of which, including two tautomeric forms  
15 of Ade, are shown in Scheme 1.



**Scheme 1.** Molecular structures of (a) 9H-Ade, (b) 7H-Ade, (c) Ado, and (d) AMP.

1           The absorption spectra of Ade, Ado and AMP are nearly identical.<sup>4</sup> The lowest  
2 absorption band centered at ~260 nm consists of overlapping bands of  $\pi\pi^*$  excitations localized  
3 on the adenine moiety,  $L_a$  (HOMO  $\rightarrow$  LUMO) and  $L_b$  (HOMO - 2  $\rightarrow$  LUMO and HOMO  $\rightarrow$   
4 LUMO + 1). Theoretical studies indicate that the  $L_a$  state carries the majority of the oscillator  
5 strength, while the close lying  $n\pi^*$  state is optically dark.<sup>3</sup> For Ade in the gas phase, the most  
6 commonly accepted relaxation mechanism is the stepwise  $S_2 (\pi\pi^*) \rightarrow S_1 (n\pi^*) \rightarrow S_0$  (gr)  
7 pathway based on biexponential decay with ultrafast (<100 fs) and slower (0.75-1.1 ps) time  
8 constants.<sup>14-19</sup> This mechanism is supported by numerous theoretical studies showing there are  
9 two conical intersections (CIs) of the excited states coupled with the ground state characterized  
10 by puckering of the pyrimidine ring at the C2 atom for the  $S_0/L_a$  CI ( ${}^2E$ ) and puckering at the  
11 C6 atom for the  $S_0/n\pi^*$  CI ( ${}^6S_1$ ).<sup>3, 20-28</sup>

12           The effect of the aqueous environment on the relaxation dynamics, on the other hand,  
13 still remains elusive in many respects. Many femtosecond time-resolved experiments have  
14 been performed for aqueous NACs containing the adenine moiety, including transient  
15 absorption (TA),<sup>2, 29-32</sup> Kerr-gated time-resolved fluorescence (KTRF),<sup>31</sup> fluorescence  
16 upconversion (FU),<sup>33-39</sup> and TRPES.<sup>40, 41</sup> Theoretical work has considered the effect of  
17 solvation on the excited state dynamics<sup>37, 42-49</sup> Although there is experimental and theoretical  
18 consensus that excited state relaxation of Ado, AMP, and 9H Ade, is complete within 1 ps,  
19 there has been disagreement on whether the initially excited  $\pi\pi^*$  state relaxes directly to the  
20 ground state or if the  $n\pi^*$  state plays a role. The differences with respect to the accepted gas  
21 phase mechanism arise because in solution, the  $n\pi^*$  state is destabilized relative to the  $\pi\pi^*$  state,  
22 so its vertical excitation energy is higher than that of the  $\pi\pi^*$  state.<sup>3, 43, 47-49</sup> Relaxation is  
23 characterized by single or multiple timescales, depending on the experiment, which raises the  
24 question of which electronic states are involved. While some NAMD studies predicted the  
25 involvement of the  $n\pi^*$  state in relaxation,<sup>44, 45</sup> others suggested from the calculations of the

1 vertical excitation energies that the  $n\pi^*$  was highly destabilized in water and thus excluded  
2 from the ultrafast relaxation.<sup>47-49</sup> Moreover, two tautomeric forms, the canonical 9H form and  
3 the 7H form, are approximately equivalent in energy in aqueous solution, so both are expected  
4 to contribute to dynamics by the UV excitation.<sup>50, 51</sup> The excited state lifetimes for 9H- and 7H-  
5 tautomers have been determined at 0.1-0.6 ps and  $\sim 9$  ps, respectively.<sup>30, 32, 35, 36, 40</sup> Based on the  
6 similarity in the obtained time constants and the structural correspondence, the dynamics of  
7 canonical 9H adenine are considered to be similar to those of Ado and AMP.<sup>2, 30, 34, 35, 40</sup>

8         These considerations motivated studies of electronic relaxation in adenine and its  
9 derivatives using liquid jet TRPES, since such an experiment can in principle detect both  $\pi\pi^*$   
10 and  $n\pi^*$  states via one-photon ionization. Experiments using UV pump and probe pulses were  
11 carried in by Lübcke<sup>40</sup> and, later, in our laboratory.<sup>41</sup> In the first study, in which aqueous Ade  
12 and Ado were excited at 4.66 eV and ionized at 5.0-5.2 eV, a monoexponential decay with a  
13 time constant of 100-215 fs depending on the ionization photon energy was obtained for Ado.  
14 For Ade, two time constants in its biexponential decay of 60-80 fs and 2-8 ps were attributed  
15 to the deexcitation of the 9H- and 7H-tautomers, respectively. The liquid jet TRPES study in  
16 our group with a probe photon energy of 6.2 eV interrogated the relaxation dynamics of Ado  
17 and AMP following the  $\pi\pi^*$  excitation at 4.69-4.97 eV, where a lifetime of  $\sim 210$ -250 fs was  
18 extracted in both systems. However, UV/UV TRPES experiments can give misleading results  
19 if the probe photon energy is too low (in both gas phase and solution) since the evolving system  
20 can drop out of the “ionization window” determined by the probe photon energy.<sup>52, 53</sup> Also,  
21 the difficulty of preparing an ultrashort UV pulse can limit the time resolution of the  
22 experimental apparatus: the instrumental response function (IRF) was  $\sim 170$  fs in the  
23 experiment with the 6.2-eV probe.

24         To address the limitation of TRPES using a UV probe, several groups have  
25 incorporated femtosecond XUV probe energies at photon energies above 20 eV into their

1 experiments. Liquid jet XUV-TRPES experiments have been reported by Suzuki,<sup>54-57</sup>  
2 Kornilov,<sup>58</sup> Chergui,<sup>59, 60</sup> and Wörner.<sup>61, 62</sup> These experiments present their own set of  
3 challenges. The probe energy is sufficient to ionize the water in addition to the much more  
4 dilute solute, so one has to take care that the weak solute pump-probe signal is not overwhelmed  
5 by water photoelectrons. In addition, unless the UV pump pulse is very weak, there are time-  
6 dependent space charge effects induced by UV ionization of the solute that can distort the  
7 TRPE spectra, particularly at long delay times.<sup>63</sup> Nonetheless, Suzuki has recently had  
8 considerable success with liquid jet XUV-TRPES and has reported a systematic study of  
9 photoexcited pyrimidine bases.<sup>54</sup>

10 Here, we carry out XUV liquid jet TRPES on Ade, Ado, and AMP using a 4.7 eV  
11 pump pulse and 22 eV probe pulse formed by high harmonic generation. A key advance in this  
12 work is the replacement of the 30  $\mu\text{m}$  diameter cylindrical liquid jet used in our previous work  
13 (and in most liquid jet photoelectron spectroscopy experiments) with a flat liquid jet run in the  
14 “gas dynamic” mode,<sup>64</sup> resulting in much better spatial overlap with the incident UV and XUV  
15 light pulses and suppressed ionization of the water vapor jacket that surrounds a liquid jet;  
16 details of flat jet operation are discussed in the following section.

17 We find that all three systems undergo decay on two timescales, 100 fs and 500 fs.  
18 Global lifetime analysis yields decay-associated spectra that indicate the faster timescale,  
19 which accounts for most of the time-dependent signal, is associated with the initially excited  
20  $\pi\pi^*$  state and the slower with the  $n\pi^*$  state. To our knowledge, these results represent the first  
21 spectroscopic observation of the  $n\pi^*$  state. In addition, we observe a long-lived signal for Ade  
22 attributed to the 7H tautomer, consistent with the interpretation of earlier UV/UV TRPES.<sup>40</sup>

## 23 **2 Experimental**

24 The experiment comprises a vacuum chamber housing the liquid jet and photoelectron  
25 spectrometer, and a beamline where the femtosecond UV and XUV pulses are generated. The

1 vacuum chamber, described in detail previously,<sup>65, 66</sup> has two differentially pumped regions:  
 2 the liquid jet region, where a flat jet is formed and collected in a liquid-N<sub>2</sub> cooled trap, and a  
 3 magnetic bottle photoelectron spectrometer.<sup>67</sup> The flat jet and XUV capabilities of the  
 4 instrument are new and are described in more detail below.

5 **Sample** Adenine (Ade, Sigma-Aldrich, 5 mM), adenosine (Ado, 7 mM), adenosine-5'-  
 6 monophosphate (AMP, 10 mM) solutions are prepared with a buffer solution at pH = 7.18 with  
 7 40 mM of Trizma HCl and 15 mM of NaOH to partially neutralize it to form buffer conditions.  
 8 25 mM NaCl is further added to suppress streaming currents and associated jet charging.<sup>68-70</sup>  
 9 Trizma has been reported to be an effective corrosion inhibitor of steel,<sup>71</sup> allowing reuse of  
 10 samples after collection in the LN<sub>2</sub>-cooled trap, in principle. An HPLC pump (Shimadzu, LC-  
 11 40i) delivers the sample solutions to the microfluidic chip from which the flat jet is formed.

12 **Liquid Flat Jet** Figure 1a shows a photograph of a flat jet in operation under typical  
 13 experimental conditions; the jet is formed using a microfluidic chip device from Micronit BV  
 14 shown in the inset.<sup>64</sup> The chip consists of three channels: a 30  $\mu\text{m}$  and two outer 50  $\mu\text{m}$  channels

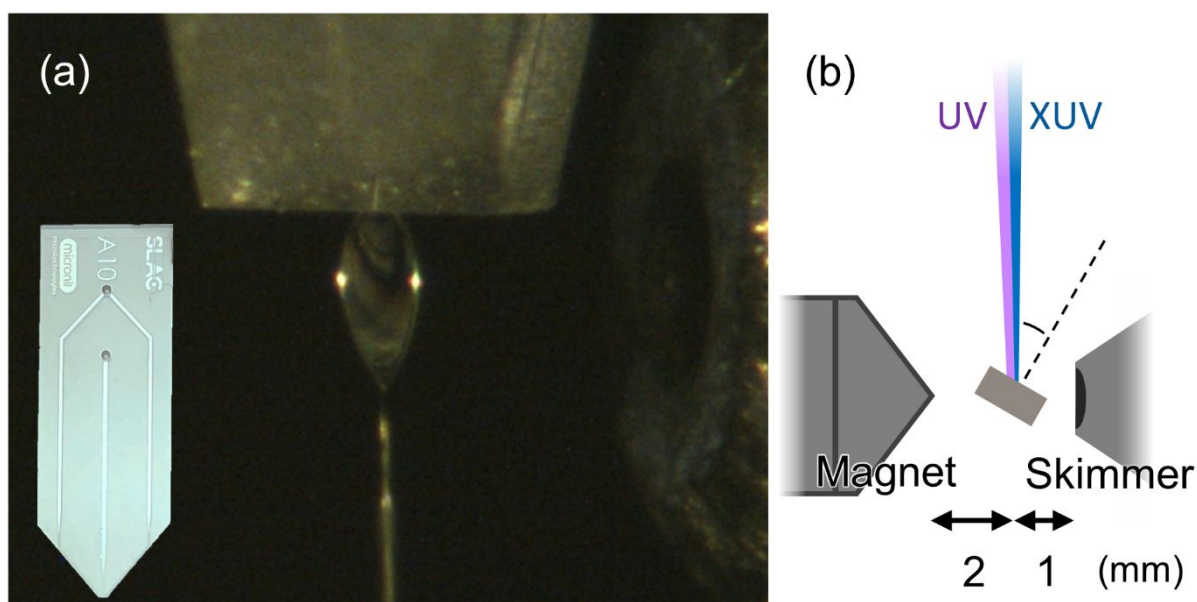


**Figure 1.** (a) Photo of gas-dynamic flat jet in operation. Inset shows the flat jet tip (Micronit) used in the experiment. (b) Schematic of the top view of the laser interaction region. The flat jet is  $\sim 1$  mm away from skimmer with a 500  $\mu\text{m}$  orifice and a magnetic cone is placed  $\sim 2$  mm away from the jet. The UV/XUV angle of incidence with the jet ( $\theta$ ) is set at 30-60° to optimize photoelectron collection efficiency.

1 that merge with the central channel at  $40^\circ$  at the tip of the jet. This device has been used by our  
2 group in molecular beam scattering experiments where a flat jet is formed by flowing liquid  
3 through the two outer channels; the central channel is not used.<sup>72, 73</sup> The flat jet thus produced  
4 in so-called “colliding-jet” geometry has been used in XUV photoelectron spectroscopy by  
5 Winter<sup>74</sup> and Suzuki.<sup>75</sup> In our TRPES experiment, we operate the flat jet in the “gas dynamic”  
6 mode, in which liquid flows through the central channel and He gas flows through the two  
7 outer channels, flattening the liquid jet and producing the image in Fig. 1a. Both the liquid flow  
8 rate and gas load on the chamber are reduced in the gas dynamic mode; other advantages are  
9 described below.

10 In normal operation, the liquid sample delivery rate is 0.2 mL/minute, controlled by  
11 the HPLC pump, and the He input gas pressure is approximately  $\sim 300$  kPa (monitored by Wika  
12 #111.11.53) to produce a stable flat jet. The flat jet image in Fig. 1a has a dimension of about  
13  $200(w) \times 500(l)$   $\mu\text{m}$  and shows a strong interference fringe, demonstrating the ultrathin ( $< 1$   $\mu\text{m}$ )  
14 nature of the sheet. This sheet size provides better spatial overlap with the pump and probe  
15 pulses than a cylindrical jet. The jet is located 1 mm away from a  $500$   $\mu\text{m}$  skimmer that serves  
16 as the entrance orifice to the magnetic bottle photoelectron spectrometer. We found that the  
17 photoelectron intensity is maximized and similar for laser/flat jet incident angles ranging from  
18  $30$ - $60^\circ$  (Fig. 1b).

19 **Femtosecond Laser Pulses** A schematic diagram for XUV-TRPES with a 266-nm (4.66-eV)  
20 pump is described in Fig. 2. A 7 mJ, 35 fs laser pulse centered at 797 nm is produced by a  
21 femtosecond regenerative amplifier system (Astrella, Coherent) operated at a repetition rate of  
22 1 kHz. The pulse is split by a set of beamsplitters. 1 mJ is delivered to a third harmonic  
23 generation setup consisting of a pair of  $\beta$ -barium borate (BBO) crystals to generate a UV pump  
24 pulse at 266 nm. Another 1 mJ is sent to a TOPAS (Coherent) that can generate tunable visible  
25 and UV light but is only used for a calibration of the photoelectron spectrometer. The remaining

1 5 mJ is frequency-doubled in a 200- $\mu\text{m}$  thick BBO crystal and any unconverted fundamental  
 2 is removed using a 1-mm thick dichroic mirror. The isolated 400-nm beam ( $900 \mu\text{J}$ ) passes  
 3 through a 1 m focal length plano-convex lens and is focused at the exit of a 60-cm semi-infinite  
 4 gas cell (SIGC)<sup>76</sup> filled with Kr gas at 3 torr, resulting in XUV light from high harmonic  
 5 generation (HHG).

6 HHG results in odd harmonics of the driving laser that are spaced by 6 eV for a 400 nm  
 7 driver. We wish to obtain spectrally pure light at 22 eV, the 7th harmonic. After the SIGC, the  
 8 light propagates through a 200-nm thick Al filter that transmits XUV harmonics above 15 eV  
 9 and blocks residual 400-nm light. The filtered XUV is then guided to a toroidal mirror at an  
 10 incident angle of  $4^\circ$  that focuses it onto the sample. Right after the toroidal mirror, the beam is  
 11 turned by  $90^\circ$  by a multilayer mirror designed by the Center for X-Ray Optics at Lawrence  
 12 Berkeley National Laboratory to selectively reflect the 7th harmonic of the 400 nm driving

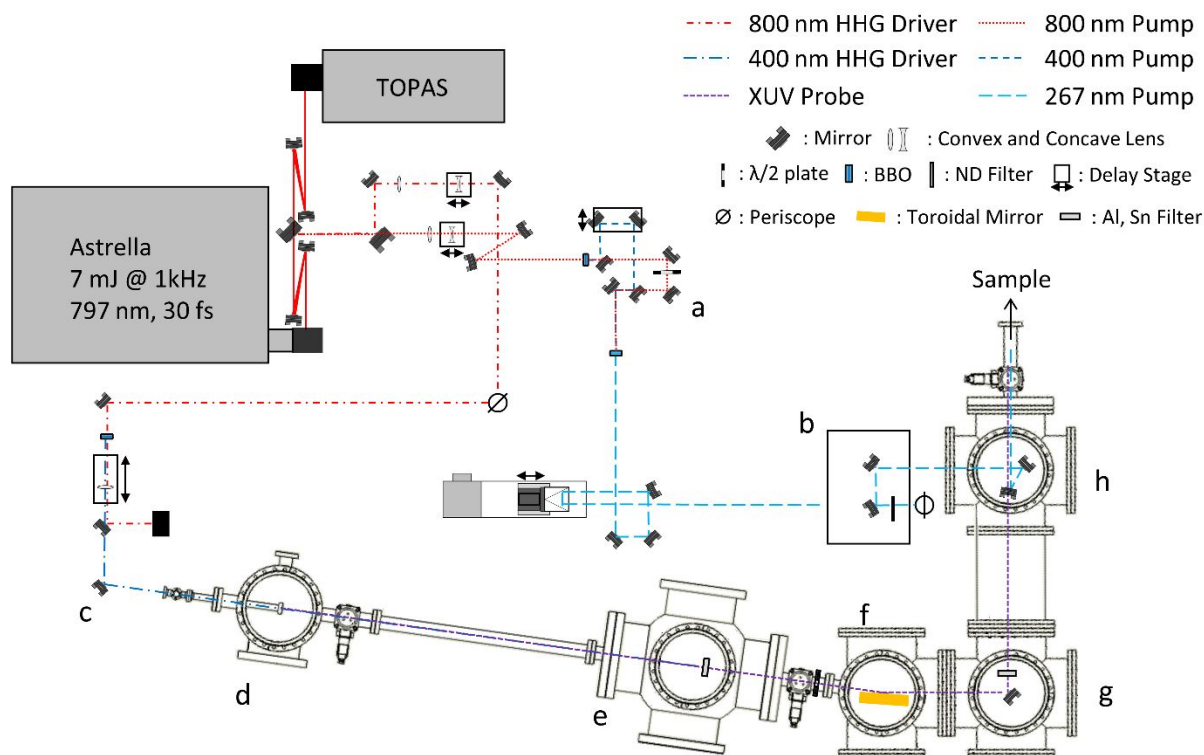


**Figure 2.** Optical setup for 266-nm pump/XUV (21.7 eV) probe experiment. Layout consists of (a) BBO-based third harmonic generation setup, (b) breadboard above table for coupling into vacuum, (c) second harmonic generation setup for HHG, (d) semi-infinite gas cell (SIGC), (e) 200-nm thick Al filter, (f) toroidal mirror, (g) multilayer mirror, and (h) annular mirror where the pump pulse is combined.

1 pulse. Residual 9th harmonic is removed by a 200-nm Sn filter downstream of the multi-layer  
2 mirror.

3 The UV pump beam is coupled into vacuum through a 2-mm CaF<sub>2</sub> window. The XUV  
4 and UV beams are combined by means of an annular concave mirror with a focal length of 1  
5 m; the XUV beam passes through the annular hole while the UV beam is reflected and focused  
6 onto the sample. This configuration enables pump-probe spatial overlap at a minimal crossing  
7 angle, approximately 0.5°. Using a curved mirror for focus instead of a convex lens also  
8 preserves temporal characteristics of the pump pulse. The IRF of the setup is evaluated by  
9 measuring the intensity of UV sidebands in the XUV photoelectron spectra of Ar, Xe, and the  
10 liquid water jet using the laser-assisted photoelectric effect (LAPE)<sup>59, 77-79</sup> and is found to be  
11 30 fs (1 $\sigma$ ). A result of LAPE measurement of H<sub>2</sub>O flat jet (NaCl 25 mM) is shown in Fig. S1.  
12 The spatial cross-correlation of pump and probe pulses is estimated at 150  $\mu$ m by tracking the  
13 Ar LAPE intensity while scanning the UV pump pulse vertically and horizontally, where the  
14 step sizes of the piezoelectric motors on the mirror controlling the pointing are calibrated by  
15 imaging the beam spot with a CMOS camera sensor (Imaging Source, DFK72BUC02). In all  
16 experiments, the UV pulse energy is at ca. 250 nJ at the sample position, while the XUV probe  
17 pulse energy is 2-5 nJ.

18

19 **Photoelectron Detection** Photoelectrons were directed by the inhomogeneous magnetic field  
20 of the magnetic bottle time-of-flight (ToF) photoelectron spectrometer comprising a stack of  
21 neodymium magnets with a soft iron cone and a solenoid maintaining 8G homogeneous field  
22 in a ~66-cm ToF tube. Photoelectrons are detected by chevron-stack microchannel plates  
23 (MCPs) coupled to a phosphor screen; the screen is used only for the alignment of the magnetic  
24 bottle. Signal pulses from the anode is amplified by a variable gain preamplifier (Stanford

1 Research Systems, SR446) before being transmitted to an ADC digitizer card (Aquiris,  
2 U5309A).

3 The observed photoelectron kinetic energy (eKE) is calibrated using Ar, for which the  
4 ionization energy of 15.76 eV,<sup>80</sup> and Xe with ionization energies of 12.13 eV for Xe<sup>+</sup> (<sup>2</sup>P<sub>3/2</sub>)  
5 and 13.44 eV for Xe<sup>+</sup> (<sup>2</sup>P<sub>1/2</sub>).<sup>81</sup> LAPE measurements of Ar are also employed with the 266-nm  
6 pump pulse, yielding more data points from the XUV + UV sidebands and thus improving the  
7 accuracy of the calibration procedure.

8 Photoelectron spectra for each time delay are acquired for over 10<sup>6</sup> shots for Ado,  
9 600,000 shots for AMP, and 650,000 shots for Ade. Because photoelectrons from the liquid-  
10 and gas-phase water are obtained simultaneously in addition to the solute pump-probe signals,  
11 the light-induced shift of the liquid peak relative to the static gas peak position is monitored in  
12 the experiment (see Section 3-b for more details).

13

### 14 **3 Results**

15

#### 16 **3a: Flat vs cylindrical liquid jet**

17 Figure 3 shows one-photon XUV (21.7 eV) photoelectron spectra of Ado aqueous solution (see  
18 Section 2) obtained with a 30 μm diameter cylindrical jet running at 1.0 mL/min through a  
19 fused-silica capillary and a flat jet with the microfluidic chip device operating in the gas  
20 dynamic mode. Spectra are plotted as a function of electron binding energy (eBE):  $eBE = h\nu_{XUV} - eKE$ .  
21 The photoelectron spectrum of the cylindrical jet shows two sharp peaks from ionization  
22 out of the 1b<sub>1</sub> (eBE = 12.5 eV) and 3a<sub>1</sub> (14.7 eV) molecular orbitals of gas phase H<sub>2</sub>O in the  
23 vapor jacket surrounding the liquid jet; the broad weaker feature at ~11.3 eV is from the 1b<sub>1</sub>  
24 orbital of liquid water. Similar spectra have been recorded by Winter and others.<sup>58, 82, 83</sup>

25 In the flat jet spectrum, the broad liquid features are considerably enhanced relative to  
26 the gas phase peaks. This is partly due to better spatial overlap between the XUV beam and the

1 flat jet. However, a comparison to the x-ray photoelectron spectrum reported by Winter on a  
2 flat jet formed by colliding two cylindrical jets shows that there is substantial suppression of  
3 the vapor features in our spectrum.<sup>74</sup> We take this to mean that in a gas-dynamic flat jet, the He  
4 sweeps away much of the vapor jacket, greatly reducing the gas phase contribution to the  
5 photoelectron spectrum. Note that He does not absorb XUV light at 21.7 eV<sup>84</sup> so there is no  
6 deleterious effect from the He side jets.

### 7 **3b: Time-dependent signals and the space-charge correction**

8 In the time-resolved measurements, relatively high photoelectron yields from both pump and  
9 probe pulses induce time-dependent space charge effects that arise as a kinetic energy shift of  
10 the probe photoelectrons from the solution.<sup>55, 58, 63</sup> As discussed by Kornilov,<sup>58</sup> the most  
11 troublesome effect of these results from pump-pulse ionization of solute molecules via resonant  
12 multiphoton ionization. Photoelectrons produced by this process are ejected into vacuum,  
13 leaving a net positive charge on the jet, and this net charge slows photoelectrons generated by  
14 the XUV pulse coming after the UV pulse. Moreover, this shift is dependent on the pump-  
15 probe delay and is larger for longer delay times. This effect must therefore be corrected in order  
16 to carry out an accurate background subtraction. To measure the shift of the liquid water  
17 features with delay time, the positions of the  $1b_{1(g)}$  and  $1b_{1(l)}$  peaks at each time delay are fit to  
18 a double-Gaussian, yielding the time-dependent space-charge shift which can be applied to the

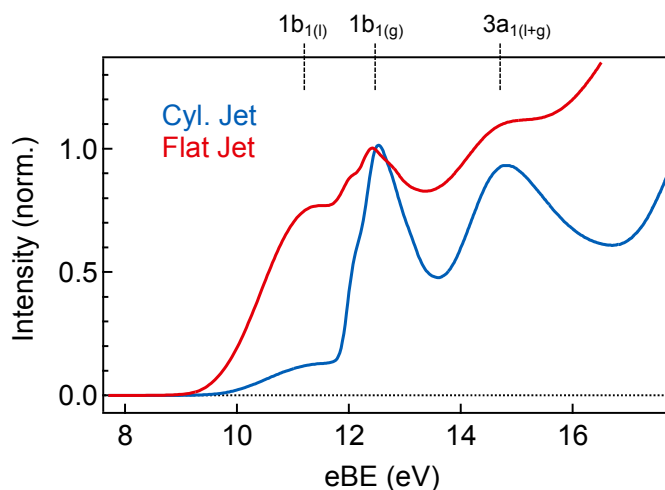


**Figure 3.** One photon photoelectron spectra of an aqueous Ado solution depending on the mode of a jet; a 30- $\mu\text{m}$  cylindrical jet (blue) and a flat jet (red).

1 TRPE spectrum at each delay time. Figure S2a shows an example of the double-Gaussian fit  
 2 and time-dependent shift for the Ado solution used in our experiments. Under the conditions  
 3 of the experiment, the shift is as high as  $-0.2$  eV at a delay of 20 ps, the longest time-delay  
 4 reported in this work (Fig. S2b).

5 Figure 4 shows spectral lineouts of space charge corrected TRPE spectra of Ado using  
 6 267 nm pump and 21.7 eV probe pulses. The validity of the space charge correction is  
 7 confirmed by the constant position of the water  $1b_{1(0)}$  peak (10-12 eV) over time. The baseline  
 8 spectrum at  $-300$  fs (black line) shows a shoulder around 7.5 eV on the tail of the liquid water  
 9 peak. The ionization potential of adenine in water has been determined experimentally to be  
 10  $7.7$  eV<sup>85</sup> and agrees well with the eBE of this feature.

11 In the time-dependent curves, the strong signal at  $t = 0$  fs from 5-8 eV is from the  
 12 LAPE sideband by the pump pulse.<sup>59</sup> The pump-probe signal, which is the main feature of  
 13 interest, is the small but discernible signal above the baseline from 3-7 eV that persists for  
 14 positive delay times.

### 15 3c: Pump-probe signals

16 Figure 5a displays a contour plot of the baseline subtracted TRPE spectra of Ado out  
 17 to 2 ps. Those of AMP and Ade are available in Fig. S3 and 4. A positive signal is observed  
 18 out to 3 eV eBE, along with an intense LAPE signal above 5 eV at the time origin. Fig. 5b

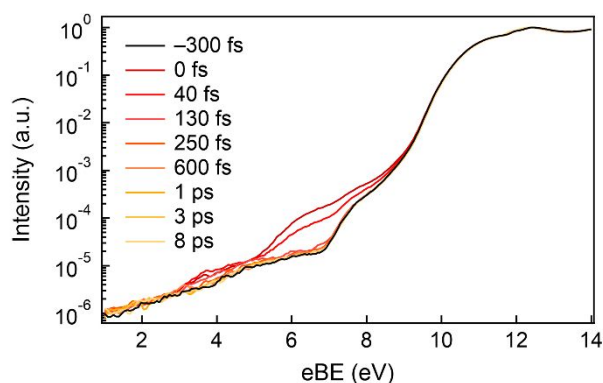


**Figure 4.** Spectral lineouts for Ado obtained using UV pump (267 nm, 250 nJ/pulse) and XUV (21.7 eV) probe with the space-charge shift corrected.

19 shows an expanded view of the lowest eBE signal at short delay times. To extract the signal

1 from the excited state of NACs, the LAPE feature is subtracted from the plot using the  
 2 procedure described in Section 4. The results are presented in Fig. 5c for Ado, 5d for AMP,  
 3 and 5e and f for Ade, respectively. Note that the contour plot for the NaCl H<sub>2</sub>O result (Fig. S1)  
 4 reproduces the same feature at  $t = 0$ . However, we do not use this result without chromophores  
 5 to subtract from the pump-probe data because the background photoelectron spectrum depends  
 6 significantly on jet conditions that are highly susceptible to the choice of solutes. Thus we  
 7 subtract the LAPE contribution by global lifetime analysis, as explained in detail in Section 4.

8 In Fig. 5b, the spectrum predominantly comprises two features: one  $<4.2$  eV and the  
 9 other from 4.2-4.7 eV. The lower eBE peak appears to shift from 3.7 to 4.0 eV within 50 fs and  
 10 the 4.0-eV feature starts to decay around 100 fs. There is a similar trend of shift in the higher  
 11 eBE feature (4.2-4.8 eV) although it is less prominent because of the overlap with the first

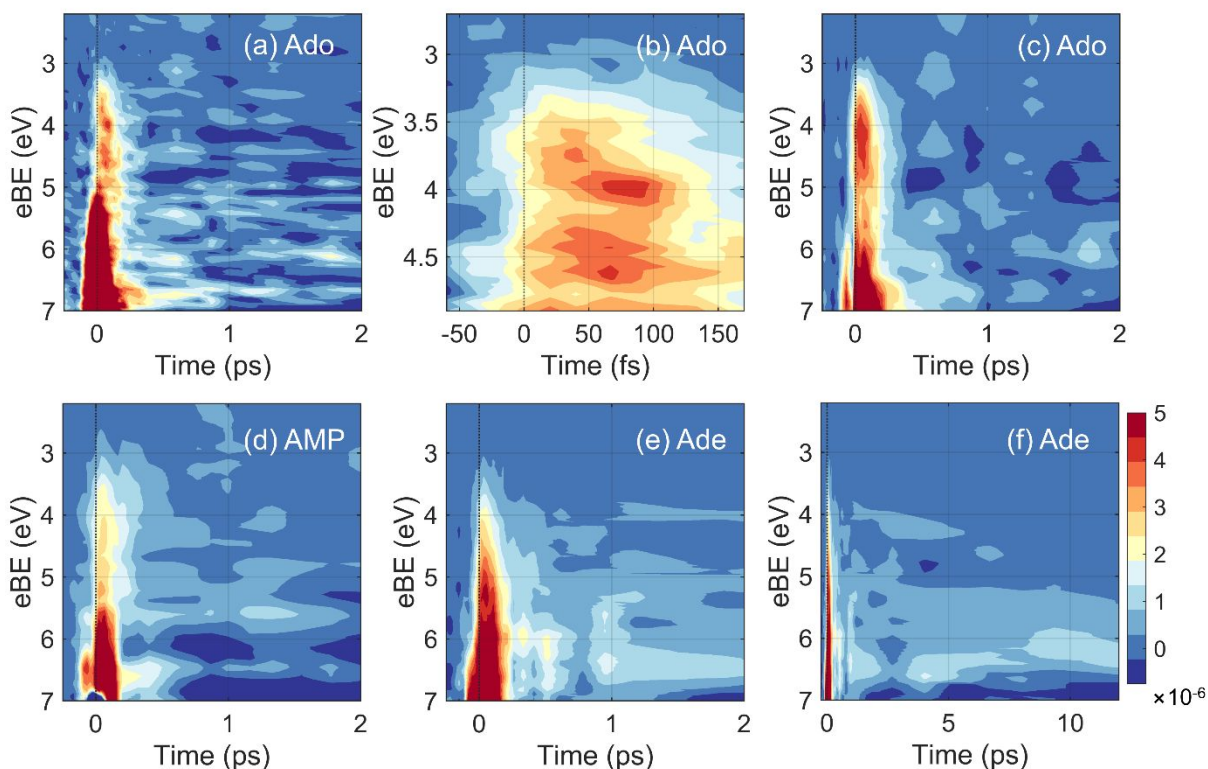


**Figure 5.** Contour plots of the baseline-subtracted pump-probe signals. (a) Ado without smoothing. (b) Expanded view of (a) around  $t = 0$ . (c-f) LAPE-subtracted TRPE spectra of (c) Ado, (d) AMP, (e,f) Ade at short and long time delays, respectively. 9-point spectral smoothing is applied to all LAPE-subtracted plots in c-f and 3-point temporal smoothing is additionally applied to the AMP data (d).

1 peak. These short-time effects, while subtle, are real and are not affected by, for example, space  
2 charge effects that are very small at short time delays (Figure S2b).

3 LAPE subtraction in Fig. 5c reveals strong signals at binding energies greater than 6  
4 eV that appear immediately after photoexcitation along with the feature at 3-5 eV. Much of the  
5 signal across the spectrum disappears by 200 fs, but signal above 5 eV persists out to 1 ps.  
6 The overall appearance of the spectrum is consistent with excited states of Ado relaxing to the  
7 ground state on an ultrafast (<1 ps) timescale. The AMP signal (Fig. 5d) is weaker but exhibits  
8 similar time evolution similar to Ado.

9 Figures 5e and f show LAPE-subtracted TRPE spectra of Ade at time delays out to 2  
10 and 12 ps, respectively. In contrast Ado and AMP, Ade signal from 5-7 eV persists out to 12  
11 ps. In contrast Ado and AMP, the intense feature of Ade does not completely decay in an  
12 ultrafast timescale. A significant portion of the signal at 4 eV remains over 5 ps, while a feature  
13 in the higher eBE region is seen throughout our detection time window.

#### 14 15 **4 Analysis**

16 To obtain an overall view of the relaxation dynamics, the background-subtracted TRPE spectra  
17 of Ado (Fig. 5a), AMP (Fig. S3), and Ade (Fig. S4) are further analyzed using Global Lifetime  
18 Analysis (GLA). In this analysis, the overall 2D dataset  $S(eBE, t)$  is expressed as a sum of  
19 exponential functions convolved with an instrumental response function  $L(t)$ :

$$20 \quad S(eBE, t) = [S_0(eBE) + \sum_{i=1}^n DAS_{\tau_i}(eBE) \cdot \exp(-t/\tau_i) + c] * L(t) \#(1)$$

21 where

$$22 \quad L(t) = \frac{1}{\sigma\sqrt{2\pi}} \exp\left(-\frac{t^2}{2\sigma^2}\right) \#(2)$$

23 In eq. (1),  $n$  is the number of time constants required for a fit. The coefficients of each  
24 exponential component are referred to as the Decay Associated Spectrum:  $DAS_{\tau_i}(eBE)$ . The

1 parameter  $c$  is the residual constant signal that represents either background noise or a very  
2 long-lived state. The prefactor  $S_0(eBE)$  represents the coherent spike due to the LAPE sideband  
3 at  $t = 0$ . Subtraction of its time profile  $S_0(eBE) \cdot L(t)$  from the dataset gives the intrinsic time  
4 evolution for the photoexcited chromophores. The analyses are performed from  $-300$  fs to 6 ps  
5 for Ado and AMP, and from  $-300$  fs to 20 ps for Ade. To improve the fitting quality, a 9-point  
6 boxcar averaging in energy is applied to all datasets. The data for AMP is further smoothed in  
7 time by three points which we confirm does not significantly alter the time profiles (Fig. S5).  
8 The LAPE-subtracted, smoothed TRPE spectra for the three NACs are shown in Figs. 5c-f.

9         For all three systems, all or most (for Ade) signal decays within 1 ps, and the number  
10 of exponential functions to reproduce each dataset is carefully and mutually considered. In all  
11 datasets within 2 ps, two time constants of at ca. 100 and 500 fs always give smaller residuals  
12 than a single time constant with ca. 150 fs, as shown in Fig. S6-9. The difference between  
13 monoexponential and biexponential fits for Ado is subtle. However, after analyzing the datasets  
14 for AMP and Ade, which exhibited significantly smaller residuals for the biexponential fit  
15 within 2 ps, we concluded that the biexponential decay better represents the dynamics.  
16 Consequently, two time constants are required to adequately fit the data set for Ado and AMP,  
17 leaving no long-lived offset above the noise level while three time constants with the positive  
18 offset component are needed for Ade to account for the overall decay. The time constants and  
19 DASs are shown in Fig. 6 for all three NACs.

1            The two DASs obtained for Ado are displayed in Fig. 6a.  $\text{DAS}\tau_1$  ( $110 \pm 10$  fs) covers  
 2 the entire spectral region of Ado with peaks at 4.0 and 4.8 eV and a slope extending towards  
 3 higher eBE. The second, relatively small,  $\text{DAS}\tau_2$  is obtained with  $470 \pm 160$  fs and exhibits  
 4 two peaks at 4.5 eV and 5.3 eV. Analysis of the single exponential decay yields a time constant  
 5 of 135 fs; in the corresponding DAS shown in Fig. S10 the two peaks seen in the red trace of  
 6 Fig. 6a are no longer distinct. The obtained fitting curves deviate from the data for eBE <4 eV  
 7 and >6 eV (see Fig. S6c and d, respectively). DASs in AMP are obtained with similar time

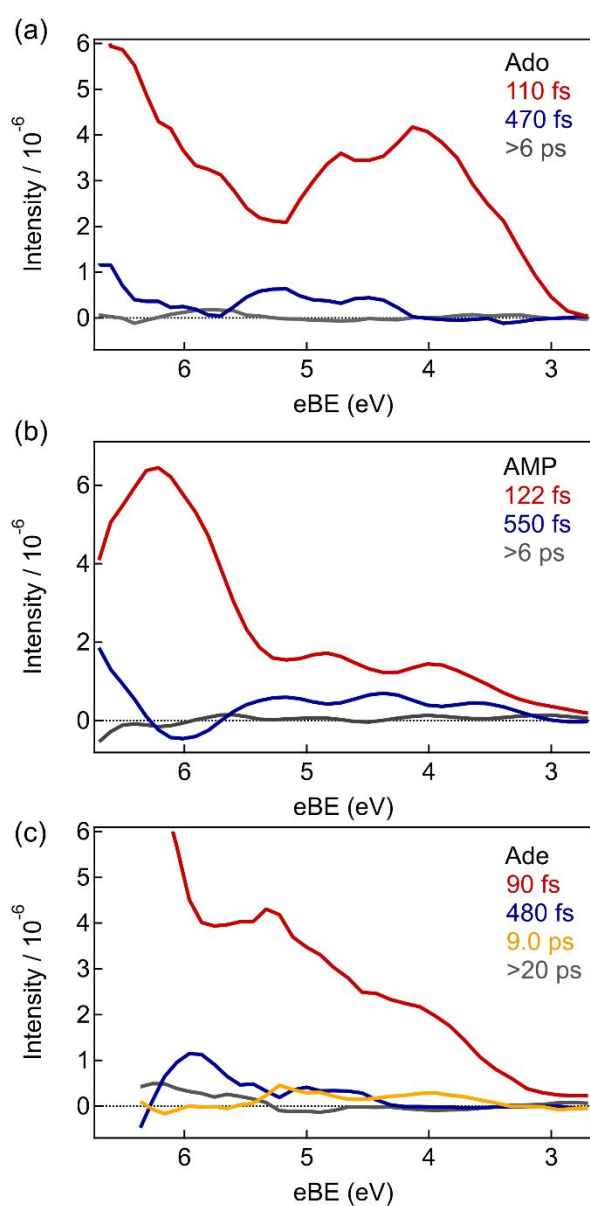


**Figure 6.** DASs obtained from GLA for (a) Ado, (b) AMP, and (c) Ade.  $\tau_i$  for each  $\text{DAS}_i$  is shown in the same color on the top right. The gray spectra represent the long-lived offset (c).

1 constants ( $\tau_1 = 122 \pm 5$  fs,  $\tau_2 = 550 \pm 50$  fs) and those spectral shapes are roughly similar;  
2 DAS $\tau_1$  has two peaks at 4.0 and 4.8 eV with a strong feature over 5 eV and DAS $\tau_2$  consists of  
3 peaks at 4.5 eV and 5.3 eV with another peak at 3.7 eV.

4 In Ade, three time constants ( $\tau_1 = 90 \pm 4$  fs,  $\tau_2 = 480 \pm 90$  fs,  $\tau_3 = 9.0 \pm 4.9$  ps) are  
5 required to fit the result out to 20 ps.  $\tau_1$  is slightly shorter than for Ado and AMP while  $\tau_2$  is  
6 the same within error bars. The third, slow component is only seen in Ade. DAS $\tau_1$  in the lower  
7 eBE region is similar to Ado and AMP, with a peak at 4.0 eV, while the shape and intensity  
8 higher than 4 eV can be distinguished with a peak at around 5.4 eV. DAS $\tau_2$  comprises two  
9 peaks at 4.8 eV and 5.8 eV. DAS $\tau_3$  has two peaks at 4.0 eV and 5.0 eV that correspond well  
10 with those in DAS $\tau_1$  of Ado and AMP. The long-lived offset (>20 ps) component has a positive  
11 onset around 6 eV, as opposed to Ado and AMP.

12

## 13 **5 Discussion**

### 14 **5a: Ado, AMP, and the short time dynamics of Ade**

15 In this study, the relaxation dynamics of adenine and its derivatives in aqueous solution are  
16 interrogated by XUV-TRPES, exploiting a high probe energy to access the complete manifold  
17 of states throughout the entire relaxation process with high temporal resolution (30 fs). These  
18 advantages allow us to assess the non-adiabatic dynamics taking place on an ultrafast  
19 timescale.<sup>86</sup> Two time constants,  $\sim 100$  and  $\sim 500$  fs, are needed to reproduce the overall  
20 evolution in Ado, AMP, and Ade within  $< 2$  ps. For Ade, we also observe a longer-lived signal  
21 that persists for  $\sim 9$  ps. A similar long-lived signal for Ade was seen in the UV/UV liquid jet  
22 TRPE spectrum by Lübcke and co-workers<sup>40</sup> and was attributed to the 7H conformer of Ade,  
23 which is expected to comprise 22% of the Ade in solution at 20°C.<sup>50, 51</sup>

24 It is instructive to compare the results here with our earlier UV/UV TRPES study of  
25 Ado and AMP using a 6.2 eV probe photon.<sup>41</sup> In that work, the effective eBE cutoff was about

1 5.5 eV, owing to poor transmission of the magnetic bottle spectrometer for electron kinetic  
2 energies below 0.7 eV. Hence, in Ado, only the lower energy feature starting around 5 eV was  
3 fully characterized, and the longer-lived signal at higher eBE was largely missed. The UV/UV  
4 data on Ado could be fit by a single exponential decay of 210 fs; the biexponential result from  
5 the XUV results reported here reflects the more complete view of the dynamics obtained at the  
6 higher probe energy and, to some extent, the improved temporal resolution of the XUV  
7 experiment.

#### 8 **5b: Assignment of the dynamics**

9 We next consider assignment of the states associated with the two decay constants, focusing  
10 first on Ado since the signals are somewhat stronger than for Ade and AMP. The initially  
11 populated excited state is safely attributable to the  $L_a$  state since it carries most of the oscillator  
12 strength.<sup>48</sup> In  $DAS\tau_1$  for Ado in Fig. 6, the lowest eBE peak at 4.0 eV thus corresponds to the  
13 ionization from the  $\pi^*$  orbital, leaving a hole on the HOMO  $\pi$  orbital ( $D_0$ ) and the second peak  
14 at  $\sim 4.8$  eV is likely due to the ionization to the second lowest  $\pi$ -hole cationic state. This splitting  
15 is consistent with previous studies of photoionization from the ground state of adenine.<sup>53, 87, 88</sup>  
16 The rising signal for eBE  $> 5$  eV in  $DAS\tau_1$  is attributed to photoionization to higher excited  
17 states of the Ado cation.

18  $DAS\tau_2$  for Ado appears to correspond to ionization from a different electronic state.  
19 It includes two peaks at 4.5 and 5.3 eV, both of which are 0.5 eV higher than the two peaks in  
20  $DAS\tau_1$ . From a theoretical study of the gas-phase photoelectron spectrum of adenine, the  
21 lowest n-hole cation is the  $D_1$  state, which is located at 0.65-1.0 eV above  $D_0$ , while the second  
22 lowest n-hole cation,  $D_3$ , is 0.4-0.7 eV above the  $D_2$  level.<sup>53</sup> Based on Koopmans' theorem,  
23 ionization from the  $\pi\pi^*$  excited state to the n-hole cation is forbidden, as is ionization from the  
24  $n\pi^*$  state to a  $\pi$ -hole cation. Thus, one can reasonably relate the alternating peak positions of  
25  $DAS\tau_1$  and  $DAS\tau_2$  to the progression of the  $D_{0-3}$  ionization series with different hole characters,

1 suggesting that  $\text{DAS}\tau_2$  corresponds to ionization out of the  $n\pi^*$  state, and that this state is  
2 responsible for the slower decay of  $\sim 500$  fs. This interpretation is consistent with the gas-phase  
3 TRPES where the peaks of the first and second DASs are separated by 1 eV and have binding  
4 energies reasonably corresponding to  $D_0$  and  $D_1$ .<sup>15</sup> The smaller energy difference between the  
5 first peaks of  $\text{DAS}\tau_1$  and  $\text{DAS}\tau_2$  in the current study is attributed to the strong destabilization  
6 of the  $n\pi^*$  state in water.<sup>3</sup> The second time constant with  $\sim 500$  fs is found in AMP and Ade as  
7 well, suggesting that the  $n\pi^*$  state participates in the dynamics independently of the sugar and  
8 phosphate group.

9         Another possibility for the longer decay component is relaxation of vibrationally hot  
10 ground state molecules formed from by passage through the  $L_a \rightarrow S_0$  CI. Based on previous UV-  
11 VIS TA and TR-IR studies,<sup>30, 32, 89-92</sup> repopulation of the thermalized ground state recovery is  
12 complete within  $\sim 2$  ps of photoexcitation for all three NACs. Pecourt et al.<sup>29</sup> calculated the  
13 initial vibrational temperature in the ground state to be  $\sim 1200$  K assuming that all the electronic  
14 energy released by internal conversion to the ground state is converted to vibrational energy  
15 that undergoes intramolecular vibrational redistribution before any cooling by the solvent.  
16 Even under this assumption, which serves as an upper bound for the ground state vibrational  
17 temperature, most vibrational modes of the Ado are not FC active and we would not expect a  
18 broadening of the ground state band by more than 1 eV.<sup>93-95</sup> Therefore, if this contribution were  
19 present, it would be expected to appear around 6-7 eV, but it is unlikely to account for the 500  
20 fs decay observed here at considerably lower eBE.

21         Finally, we consider the earliest dynamics shown in Fig. 5b, where peak shifts within  
22 100 fs are displayed. These rapid variations in the TRPE spectra are most likely from  
23 wavepacket dynamics near the FC region on the initially excited  $L_a$  state. We attribute these  
24 early dynamics to wavepacket propagation on the repulsive potential accessed by  
25 photoexcitation, while the decay of these signals at  $\sim 100$  fs is from  $L_a$  depopulation.

1 From this analysis and the GLA results, we conclude that the overall relaxation  
2 dynamics are similar among Ado, AMP and 9H Ade. It is expected that a transition to the  $n\pi^*$   
3 state occurs near the FC region. This transition may contribute to the dynamics in Fig. 5b but  
4 no quantitative signature for this process can be extracted.

### 5 **5c: Comparison to previous results**

6 The main result of this work is that the sub-ps dynamics of Ade, Ado, and AMP are better fit  
7 by a biexponential decay with time constants of around 100 and 500 fs than by a single time  
8 constant, and that the slower decay is associated with the  $n\pi^*$  state. It is useful to compare  
9 our results with previous experiments, summarized in Table S1. While some of these  
10 experiments report only a single time constant, typically 200-300 fs, several experiments of  
11 TA and time-resolved fluorescence report biexponential decay with time constants similar to  
12 those found here.<sup>31, 34, 35</sup> Hence, the observation of biexponential sub-ps decay appears to be  
13 reasonable, raising the question of which electronic states are involved in the overall dynamics.

14 Kwok et al<sup>31</sup> attributed their measured time constants of 130 and 450 fs time to decay  
15 of the  $L_a$  and  $L_b$  states, respectively. Gustavsson et al<sup>37</sup> also observed multiple timescales  
16 depending on the fluorescence wavelength and proposed a different mechanism in which the  
17 faster time constant is assigned to rapid wavepacket motion in the steep FC region of the  $L_a$   
18 state and the slower to  $L_a \rightarrow S_0$  internal conversion, with the  $n\pi^*$  state playing no role in the  
19 dynamics. This interpretation was based on LR-PCM/PBE0 calculations on 9H-Ade-4H<sub>2</sub>O,  
20 which predict a decreased fluorescence oscillator strength as the nucleobase geometry in the  
21  $L_a$  state evolves from planer to the non-planer C2-puckered geometry. In our XUV-TRPES  
22 experiment, the DAS for the slow time constant points to ionization out of the  $n\pi^*$  state,  
23 providing yet another interpretation of the biexponential dynamics, one based on an assigned  
24 spectral fingerprint of the  $n\pi^*$  state. Furthermore, we believe the rapid wavepacket motion on  
25 the  $L_a$  state proposed by Gustavsson et al<sup>37</sup> is observed here in Fig. 5a, where the early-time

1 wavepacket dynamics can be distinguished from the subsequent  $\sim 100$  fs decay attributed to  $L_a$   
2 deexcitation.

3 One then has to consider whether this interpretation is reasonable in the light of  
4 previous theoretical and experimental work on adenine and its derivatives. From an  
5 experimental perspective, one might argue that since the  $n\pi^*$  state is nominally optically dark,  
6 it should not contribute to the signals in FU experiments. However, our proposed identification  
7 of the  $n\pi^*$  state does not contradict previous experimental results. There are several  
8 experimental and theoretical indications that this state is mixed with the bright  $\pi\pi^*$  state. In the  
9 gas phase, resonant two photon ionization and laser induced fluorescence detected strong peaks  
10 below the 0-0 band of the  $\pi\pi^*$  state.<sup>96-98</sup> The calculation by Broo<sup>99</sup> suggested that out-of-plane  
11 distortion in 9H-Ade not only couples the  $\pi\pi^*$  to the  $n\pi^*$  state, but also leads to increased FC  
12 factors for internal conversion to the ground state, which supports the  $n\pi^*$  as an essential factor  
13 for the ultrafast decay of this molecule. In solution, Cohen<sup>30</sup> and Pancur<sup>36</sup> proposed that the N7  
14 lone pair taking part in the  $n\pi^*$  state plays a decisive role in the ultrafast decay to account for  
15 the sub-10 ps lifetime in the 7-substitution of Ade. The contribution of the N7 lone pair in the  
16  $n$  hole was confirmed in many theoretical studies.<sup>3, 28, 48</sup>

17 From a theoretical perspective, although there is consensus that the vertical excitation  
18 energy of the  $n\pi^*$  state is above the  $\pi\pi^*$  state in solution,<sup>3</sup> the role of this state in the dynamics  
19 of photoexcited Ade and its derivatives is still controversial. A semiempirical QM/MM study  
20 for aqueous 9H Ade by Thiel and co-workers<sup>45</sup> found strong mixing of the  $n\pi^*$  and  $\pi\pi^*$  state  
21 near the FC region, leading to the ultrafast  $S_2 \rightarrow S_1$  transition with 40 fs. The populated  $S_1$   
22 state acquires a predominant  $n\pi^*$  character, returning to the ground state mainly through the  ${}^6S_1$   
23 CI within 430 fs, while a small contribution of  ${}^2E$  ( $L_a/S_0$ ) CI pathway is also obtained. Mitrić  
24 suggested a similar, stepwise decay mechanism in the TD-DFTB surface-hopping simulations

1 for microsolvated adenine.<sup>44</sup> A CASSCF study of aqueous 9H Ade instead suggested partial  
 2 involvement of the  $L_b$  state in relaxation through vibronic coupling with the  $L_a$  state that had a  
 3 very small energy difference ( $<0.2$  eV).<sup>43</sup> This mechanism, however, cannot explain the large  
 4 gap between the peaks of the first and second DAS in our experiment. They also report that the  
 5  $n\pi^*$  is the lowest in energy in the nonplanar geometry and is, in principle, accessible from the  
 6  $L_a$  state through a relatively small activation barrier of 0.15 eV, although they exclude this  
 7 process because the amplitude of the wavepacket propagating at this direction is considered to  
 8 be small.

9 Based on our results and the above considerations, we propose schematic potential  
 10 energy surfaces associated with the relaxation as depicted in Fig. 7. Although the energy of the  
 11  $n\pi^*$  state at the FC region is high in aqueous media, it can be populated through a curve crossing  
 12 from the  $L_a$  state at lower energy. The reaction coordinate through the  ${}^2E$   $L_a/S_0$  CI mainly  
 13 involves C2 puckering while C6 puckering leads to relaxation through  ${}^6S_1$  CI ( $n\pi^*/S_0$ ). It is  
 14 unclear what fraction of the excited wavepacket propagates through this relaxation path in lieu

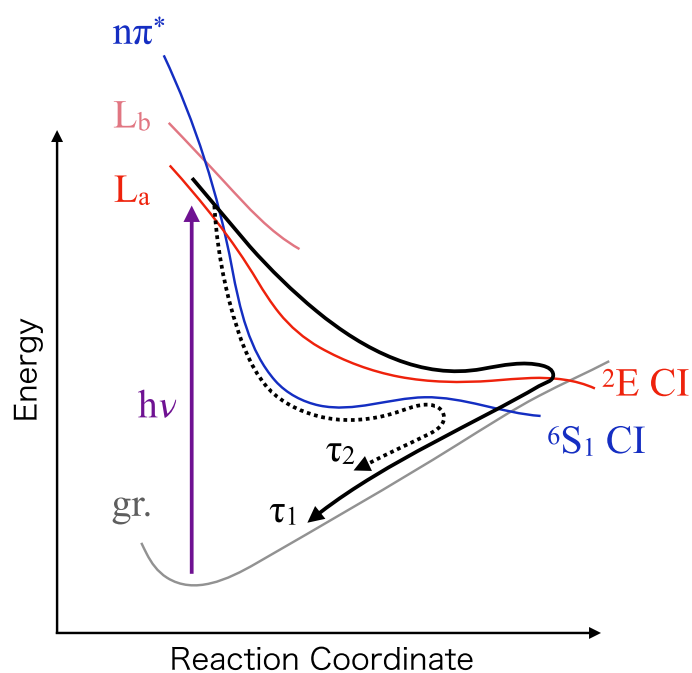


**Figure 7.** Schematic potential energy diagram for the three lowest excited states as a function of the reaction coordinate. The direct ( $L_a$  to  $S_0$ ) decay path is represented as the solid arrow and the stepwise path ( $L_a \rightarrow n\pi^* \rightarrow S_0$ ) as the dotted arrow.

1 of the direct deexcitation through the  $^2E$  CI,<sup>3</sup> and what determines the fate of the wavepacket.  
2 Based on the relative DAS intensity, direct relaxation through  $^2E$  CI appears to be the main  
3 channel and the detour through the  $n\pi^*$  is minor, assuming that the ionization cross-sections  
4 are similar between the two excited states as is the case for pyrimidine nucleobases.<sup>54</sup> Further  
5 theoretical treatment with a full solvation model would provide a better understanding of the  
6 mechanism in aqueous media.

#### 7 **5d: Assignment of the excited state dynamics of Ade**

8 As shown in the introduction, Ade forms two tautomers in the ground state: Ade9H and  
9 Ade7H.<sup>50, 51</sup> The GLA for Ade yields time constants of 90 fs, 480 fs, and 9 ps. The slowest  
10 time constant has been observed in and is consistently attributed to the excited state lifetime of  
11 7H Ade, while the fast time constants can mainly be associated with 9H Ade, in line with the  
12 other time-resolved experiments such as UV-TRPES,<sup>40</sup> TA,<sup>32</sup> and FU<sup>35, 36</sup> on aqueous adenine.  
13 This assignment was confirmed by the methylation, where 7-methyladenine exhibited the sub-  
14 10 ps excited state lifetime.<sup>30</sup> The only difference we have found here compared to previous  
15 works is the presence of the second time scale of 480 fs, attributed to the  $n\pi^*$  of 9H Ade. This  
16 interpretation is consistent with previous work, as discussed above, proposing that the  $n\pi^*$  state  
17 associated with the N7 lone pair plays a decisive role in the ultrafast decay of 9H Ade, Ado,  
18 and AMP.<sup>30, 36, 99</sup>

19 The DAS associated with the 9 ps decay can shed some light on the excited state  
20 responsible for this decay. Specifically, it exhibits a peak around 4 eV which has been assigned  
21 above to ionization to the cationic  $D_0$  state with a  $\pi$  hole, suggesting that the long-lived state of  
22 7H Ade has at least some  $\pi\pi^*$  character.

23 Within our experimental timeframe of 20 ps, GLA shows that Ade also exhibits a non-  
24 zero offset beyond the 9 ps decay of  $DAS\tau_3$ . This observation, seen for Ade but not Ado or  
25 AMP, can be explained by the phosphorescence of Ade, which is strong in 7-methyladenine

1 but is a few orders of magnitude smaller in Ado.<sup>100</sup> Therefore, the offset band in this study is  
2 attributed to the triplet state of 7H Ade. A DFT/MRCI calculation conducted on isolated 7H  
3 Ade predicts a dense manifold of low-lying triplet states in the energy regime between the FC  
4 region and the S<sub>1</sub> global minimum.<sup>101</sup> This enables intersystem crossing through multiple El  
5 Sayed-rule-allowed pathways of  $^1\pi\pi^*/^3n\pi^*$  and  $^1n\pi^*/^3\pi\pi^*$ . Some TA studies associate the long-  
6 lived signals with the two-photon ionization of Ade or water.<sup>30, 32, 90</sup> The current experiment  
7 does not find any evidence of the process, as there is no signal in the long time delay around  
8 3.7 eV where the hydrated electron band would be expected.<sup>102</sup>

9

## 10 **6 Conclusion**

11 This study investigates the ultrafast UV-induced dynamics of Ade, Ado, and AMP in aqueous  
12 solution using XUV-TRPES with a 266 nm (4.66 eV) pump pulse and a 21.7 eV probe pulse.  
13 A gas dynamic flat liquid jet is incorporated to form a flat liquid surface approximately 200  
14  $\mu\text{m}$  wide, which provides a larger exposure area to the laser focal spots. This significantly  
15 enhances the photoelectron signal from the liquid compared to that obtained by the cylindrical  
16 jet. Additionally, the helium gas jet utilized to create the flat jet removes much of the water  
17 vapor surrounding the liquid, resulting in the suppression of unwanted gas peak background.

18 The excited state signals are clearly identified in the 3-7 eV eBE range for all three  
19 NACs. Ado and AMP exhibit signals with ultrafast decays that completely merge with the  
20 baseline level within 1 ps, whereas long lived signals that can persist over 20 ps are detected  
21 in Ade. To reproduce the obtained datasets, GLA is used, which requires two time constants at  
22 approximately 100 and 500 fs for Ado and AMP. While the first DAS with distinct peaks at  
23 4.0 and 4.8 eV is safely attributed to the L<sub>a</sub> state, the second DAS consists of peaks at  $\sim 0.5$  eV  
24 lower than those of the first DAS, indicating that the  $n\pi^*$  state contributes to the relaxation  
25 dynamics. Analysis of the signal appearance time as a function of eBE suggests that the

1 wavepacket moves along a steep potential energy surface from the FC region in less than 100  
2 fs. GLA in Ade yields three time constants, where the first two components at 90 and 480 fs  
3 are safely attributable to the 9H Ade relaxation through the similar mechanisms as that of Ado  
4 and AMP, and the 9-ps component is due to the excited state of 7H Ade. Further theoretical  
5 studies under a full solvation model will be required to map out the entire relaxation pathways.  
6 This study showcases the ability of XUV-TRPES to disentangle nonadiabatic dynamics in the  
7 condensed phase and provide new insights into DNA photophysics on ultrafast timescales.

8

### 9 **Conflicts of interest**

10 There are no conflicts of interest to declare.

11

### 12 **Acknowledgments**

13 This research is supported by the National Science Foundation Division of Chemistry under  
14 Grant No. CHE-2154629 and by CALSOLV, the center for solvation studies at the University  
15 of California, Berkeley. M.K. also acknowledges the support from the Japan Society for the  
16 Promotion of Science (JSPS) Overseas Research Fellowships. D.H.K. acknowledges Basic  
17 Science Research Program through the National Research Foundation of Korea (NRF)  
18 funded by the Ministry of Education with Grant No. RS-2023-00241698. P.M. and M. H.  
19 acknowledge the support by the Deutsche Forschungsgemeinschaft (DFG, German Research  
20 Foundation) under Germany's Excellence Strategy — EXC 2033-390677874 — RESOLV.  
21 The authors thank W. Yang for his help in implementing the flat jet.

22

1 **References**

- 2  
3  
4 1. C. T. Middleton, K. de La Harpe, C. Su, Y. K. Law, C. E. Crespo-Hernández and B.  
5 Kohler, *Annu. Rev. Phys. Chem.*, 2009, **60**, 217-239.
- 6 2. C. E. Crespo-Hernández, B. Cohen, P. M. Hare and B. Kohler, *Chem. Rev.*, 2004, **104**,  
7 1977-2020.
- 8 3. R. Improta, F. Santoro and L. Blancafort, *Chem. Rev.*, 2016, **116**, 3540-3593.
- 9 4. D. Voet, W. Gratzner, R. Cox and P. Doty, *Biopolymers: Original Research on*  
10 *Biomolecules*, 1963, **1**, 193-208.
- 11 5. M. Shukla and J. Leszczynski, *J. Biomol. Struct. Dyn.*, 2007, **25**, 93-118.
- 12 6. J. Cadet, S. Mouret, J. L. Ravanat and T. Douki, *Photochem. Photobiol.*, 2012, **88**,  
13 1048-1065.
- 14 7. J.-L. Ravanat, T. Douki and J. Cadet, *J. Photochem. Photobiol. B Biol.*, 2001, **63**, 88-  
15 102.
- 16 8. R. P. Sinha and D.-P. Häder, *Photochem. Photobiol. Sci.*, 2002, **1**, 225-236.
- 17 9. M. Koga, M. Asplund and D. M. Neumark, *J. Chem. Phys.*, 2022, **156**, 244302.
- 18 10. R. P. Rastogi, Richa, A. Kumar, M. B. Tyagi and R. P. Sinha, *J. Nucleic Acids*, 2010,  
19 **2010**, 592980.
- 20 11. M. Asplund, M. Koga, Y. J. Wu and D. M. Neumark, *J. Chem. Phys.*, 2024, **160**,  
21 054301.
- 22 12. C. Sagan, *J. Theor. Biol.*, 1973, **39**, 195-200.
- 23 13. V. G. Stavros and J. R. Verlet, *Annu. Rev. Phys. Chem.*, 2016, **67**, 211-232.
- 24 14. H. Kang, B. Jung and S. K. Kim, *J. Chem. Phys.*, 2003, **118**, 6717-6719.
- 25 15. S. Ullrich, T. Schultz, M. Z. Zgierski and A. Stolow, *Phys. Chem. Chem. Phys.*, 2004,  
26 **6**, 2796-2801.
- 27 16. C. Canuel, M. Mons, F. Piuzzi, B. Tardivel, I. Dimicoli and M. Elhanine, *J. Chem.*

- 1           *Phys.*, 2005, **122**, 074316.
- 2   17.   H. Satzger, D. Townsend, M. Z. Zgierski, S. Patchkovskii, S. Ullrich and A. Stolow,  
3           *Proc. Natl. Acad. Sci. U.S.A.*, 2006, **103**, 10196-10201.
- 4   18.   C. Z. Bisgaard, H. Satzger, S. Ullrich and A. Stolow, *ChemPhysChem*, 2009, **10**, 101-  
5           110.
- 6   19.   N. L. Evans and S. Ullrich, *J. Phys. Chem. A*, 2010, **114**, 11225-11230.
- 7   20.   S. Perun, A. L. Sobolewski and W. Domcke, *J. Am. Chem. Soc.*, 2005, **127**, 6257-6265.
- 8   21.   S. Perun, A. L. Sobolewski and W. Domcke, *Chem. Phys.*, 2005, **313**, 107-112.
- 9   22.   L. Serrano-Andrés, M. Merchán and A. C. Borin, *Proc. Natl. Acad. Sci. U.S.A.*, 2006,  
10           **103**, 8691-8696.
- 11   23.   L. Serrano-Andrés, M. Merchán and A. C. Borin, *Chem. Eur. J.*, 2006, **12**, 6559-6571.
- 12   24.   M. Barbatti and H. Lischka, *J. Am. Chem. Soc.*, 2008, **130**, 6831-6839.
- 13   25.   I. Conti, M. Garavelli and G. Orlandi, *J. Am. Chem. Soc.*, 2009, **131**, 16108-16118.
- 14   26.   M. Barbatti, A. J. A. Aquino, J. J. Szymczak, D. Nachtigallová, P. Hobza and H.  
15           Lischka, *Proc. Natl. Acad. Sci. U.S.A.*, 2010, **107**, 21453-21458.
- 16   27.   M. Barbatti, Z. Lan, R. Crespo-Otero, J. J. Szymczak, H. Lischka and W. Thiel, *J. Chem.*  
17           *Phys.*, 2012, **137**, 22A503.
- 18   28.   S. Mandal and V. Srinivasan, *J. Phys. Chem. B*, 2022, **126**, 7077-7087.
- 19   29.   J.-M. L. Pecourt, J. Peon and B. Kohler, *J. Am. Chem. Soc.*, 2001, **123**, 10370-10378.
- 20   30.   B. Cohen, P. M. Hare and B. Kohler, *J. Am. Chem. Soc.*, 2003, **125**, 13594-13601.
- 21   31.   W.-M. Kwok, C. Ma and D. L. Phillips, *J. Am. Chem. Soc.*, 2006, **128**, 11894-11905.
- 22   32.   G. M. Roberts, H. J. Marroux, M. P. Grubb, M. N. Ashfold and A. J. Orr-Ewing, *J.*  
23           *Phys. Chem. A*, 2014, **118**, 11211-11225.
- 24   33.   J. Peon and A. H. Zewail, *Chem. Phys. Lett.*, 2001, **348**, 255-262.
- 25   34.   D. Onidas, D. Markovitsi, S. Marguet, A. Sharonov and T. Gustavsson, *J. Phys. Chem.*

- 1            *B*, 2002, **106**, 11367-11374.
- 2    35.    T. Gustavsson, A. Sharonov, D. Onidas and D. Markovitsi, *Chem. Phys. Lett.*, 2002,  
3            **356**, 49-54.
- 4    36.    T. Pancur, N. K. Schwalb, F. Renth and F. Temps, *Chem. Phys.*, 2005, **313**, 199-212.
- 5    37.    T. Gustavsson, N. Sarkar, I. Vaya, M. C. Jimenez, D. Markovitsi and R. Improta,  
6            *Photochem. Photobiol. Sci.*, 2013, **12**, 1375-1386.
- 7    38.    M. C. Stuhldreier and F. Temps, *Faraday Discuss.*, 2013, **163**, 173-188.
- 8    39.    T. Gustavsson and D. Markovitsi, *Acc. Chem. Res.*, 2021, **54**, 1226-1235.
- 9    40.    F. Buchner, H. H. Ritze, J. Lahl and A. Lübcke, *Phys. Chem. Chem. Phys.*, 2013, **15**,  
10           11402-11408.
- 11   41.    H. L. Williams, B. A. Erickson and D. M. Neumark, *J. Chem. Phys.*, 2018, **148**, 194303.
- 12   42.    B. Mennucci, A. Toniolo and J. Tomasi, *J. Phys. Chem. A*, 2001, **105**, 4749-4757.
- 13   43.    S. Yamazaki and S. Kato, *J. Am. Chem. Soc.*, 2007, **129**, 2901-2909.
- 14   44.    R. Mitric, U. Werner, M. Wohlgemuth, G. Seifert and V. Bonacic-Koutecky, *J. Phys.*  
15           *Chem. A*, 2009, **113**, 12700-12705.
- 16   45.    Z. Lan, Y. Lu, E. Fabiano and W. Thiel, *ChemPhysChem*, 2011, **12**, 1989-1998.
- 17   46.    Y. Lu, Z. Lan and W. Thiel, *J. Comput. Chem.*, 2012, **33**, 1225-1235.
- 18   47.    F. Santoro, R. Improta, T. Fahleson, J. Kauczor, P. Norman and S. Coriani, *J. Phys.*  
19           *Chem. Lett.*, 2014, **5**, 1806-1811.
- 20   48.    S. K. Khani, R. Faber, F. Santoro, C. Hattig and S. Coriani, *J. Chem. Theory Comput.*,  
21           2019, **15**, 1242-1254.
- 22   49.    V. Ludwig, Z. M. da Costa, M. S. do Amaral, A. C. Borin, S. Canuto and L. Serrano-  
23           Andrés, *Chem. Phys. Lett.*, 2010, **492**, 164-169.
- 24   50.    M. Dreyfus, G. Dodin, O. Bensaude and J. Dubois, *J. Am. Chem. Soc.*, 1975, **97**, 2369-  
25           2376.

- 1 51. M. T. Chenon, R. J. Pugmire, D. M. Grant, R. P. Panzica and L. B. Townsend, *J. Am.*  
2 *Chem. Soc.*, 1975, **97**, 4636-4642.
- 3 52. H. R. Hudock, B. G. Levine, A. L. Thompson, H. Satzger, D. Townsend, N. Gador, S.  
4 Ullrich, A. Stolow and T. J. Martínez, *J. Phys. Chem. A*, 2007, **111**, 8500-8508.
- 5 53. M. Barbatti and S. Ullrich, *Phys. Chem. Chem. Phys.*, 2011, **13**, 15492-15500.
- 6 54. Y. Miura, Y.-i. Yamamoto, S. Karashima, N. Orimo, A. Hara, K. Fukuoka, T. Ishiyama  
7 and T. Suzuki, *J. Am. Chem. Soc.*, 2023, **145**, 3369-3381.
- 8 55. C. W. West, J. Nishitani, C. Higashimura and T. Suzuki, *Mol. Phys.*, 2021, **119**,  
9 e1748240.
- 10 56. N. Orimo, Y.-i. Yamamoto, S. Karashima, A. Boyer and T. Suzuki, *J. Phys. Chem. Lett.*,  
11 2023, **14**, 2758-2763.
- 12 57. S. Karashima, Y.-I. Suzuki, Y.-i. Yamamoto and T. Suzuki, *Bull. Chem. Soc. Jpn.*, 2023,  
13 **97**, uoad012.
- 14 58. J. Hummert, G. Reitsma, N. Mayer, E. Ikonnikov, M. Eckstein and O. Kornilov, *J. Phys.*  
15 *Chem. Lett.*, 2018, **9**, 6649-6655.
- 16 59. C. Arrell, J. Ojeda, L. Mewes, J. Grilj, F. Frassetto, L. Poletto, F. Van Mourik and M.  
17 Chergui, *Phys. Rev. Lett.*, 2016, **117**, 143001.
- 18 60. J. Ojeda, C. A. Arrell, L. Longetti, M. Chergui and J. Helbing, *Phys. Chem. Chem.*  
19 *Phys.*, 2017, **19**, 17052-17062.
- 20 61. C. Wang, M. D. Waters, P. Zhang, J. Suchan, V. Svoboda, T. T. Luu, C. Perry, Z. Yin,  
21 P. Slaviček and H. J. Wörner, *Nat. Chem.*, 2022, **14**, 1126-1132.
- 22 62. I. Jordan, M. Huppert, D. Rattenbacher, M. Peper, D. Jelovina, C. Perry, A. Von Conta,  
23 A. Schild and H. J. Wörner, *Science*, 2020, **369**, 974-979.
- 24 63. R. Al-Obaidi, M. Wilke, M. Borgwardt, J. Metje, A. Moguilevski, N. Engel, D.  
25 Tolksdorf, A. Raheem, T. Kampen and S. Mähl, *New J. Phys.*, 2015, **17**, 093016.

- 1 64. J. D. Koralek, J. B. Kim, P. Brůža, C. B. Curry, Z. Chen, H. A. Bechtel, A. A. Cordones,  
2 P. Sperling, S. Toleikis, J. F. Kern, S. P. Moeller, S. H. Glenzer and D. P. DePonte,  
3 *Nat. Commun.*, 2018, **9**, 1353.
- 4 65. M. H. Elkins, H. L. Williams and D. M. Neumark, *J. Chem. Phys.*, 2015, **142**, 234501.
- 5 66. M. H. Elkins, H. L. Williams and D. M. Neumark, *J. Chem. Phys.*, 2016, **144**, 184503.
- 6 67. P. Kruit and F. H. Read, *J. Phys. E*, 1983, **16**, 313-324.
- 7 68. N. Preissler, F. Buchner, T. Schultz and A. Lübcke, *J. Phys. Chem. B*, 2013, **117**, 2422-  
8 2428.
- 9 69. N. Kurahashi, S. Karashima, Y. Tang, T. Horio, B. Abulimiti, Y.-I. Suzuki, Y. Ogi, M.  
10 Oura and T. Suzuki, *J. Chem. Phys.*, 2014, **140**, 174506.
- 11 70. M. Faubel, B. Steiner and J. P. Toennies, *J. Chem. Phys.*, 1997, **106**, 9013-9031.
- 12 71. B. A. Abd-El-Nabey, S. El-Housseiny and M. A. Abd-El-Fatah, *Sci. Rep.*, 2022, **12**,  
13 15346.
- 14 72. C. Lee, M. N. Pohl, I. A. Ramphal, W. Yang, B. Winter, B. Abel and D. M. Neumark,  
15 *J. Phys. Chem. A*, 2022, **126**, 3373-3383.
- 16 73. W. Yang, C. Lee, S. Saric, M. N. Pohl and D. M. Neumark, *J. Chem. Phys.*, 2023, **159**.
- 17 74. D. Stemer, T. Buttersack, H. Haak, S. Malerz, H. C. Schewe, F. Trinter, K. Mudryk, M.  
18 Pugini, B. Credidio, R. Seidel, U. Hergenbahn, G. Meijer, S. Thürmer and B. Winter,  
19 *J. Chem. Phys.*, 2023, **158**, 234202.
- 20 75. Y.-i. Yamamoto, H. Yano, S. Karashima, R. Uenishi, N. Orimo, J. Nishitani and T.  
21 Suzuki, *Bull. Chem. Soc. Jpn.*, 2023, **96**, 938-942.
- 22 76. J. P. Brichta, M. C. H. Wong, J. B. Bertrand, H. C. Bandulet, D. M. Rayner and V. R.  
23 Bhardwaj, *Phys. Rev. A*, 2009, **79**, 033404.
- 24 77. L. Miaja-Avila, C. Lei, M. Aeschlimann, J. Gland, M. Murnane, H. Kapteyn and G.  
25 Saathoff, *Phys. Rev. Lett.*, 2006, **97**, 113604.

- 1 78. T. Glover, R. Schoenlein, A. Chin and C. Shank, *Phys. Rev. Lett.*, 1996, **76**, 2468.
- 2 79. G. Saathoff, L. Miaja-Avila, M. Aeschlimann, M. M. Murnane and H. C. Kapteyn, *Phys.*  
3 *Rev. A*, 2008, **77**, 022903.
- 4 80. I. Velchev, W. Hogervorst and W. Ubachs, *J. Phys. B: At. Mol. Opt. Phys.*, 1999, **32**,  
5 L511.
- 6 81. R. D. Knight and L.-g. Wang, *J. Opt. Soc. Am. B*, 1985, **2**, 1084-1087.
- 7 82. B. Winter, R. Weber, W. Widdra, M. Dittmar, M. Faubel and I. Hertel, *J. Phys. Chem.*  
8 *A*, 2004, **108**, 2625-2632.
- 9 83. S. Thürmer, S. Malerz, F. Trinter, U. Hergenhahn, C. Lee, D. M. Neumark, G. Meijer,  
10 B. Winter and I. Wilkinson, *Chem. Sci.*, 2021, **12**, 10558-10582.
- 11 84. W. C. Martin, *J. Phys. Chem. Ref. Data*, 1973, **2**, 257-266.
- 12 85. C. A. Schroeder, E. Pluharova, R. Seidel, W. P. Schroeder, M. Faubel, P. Slavicek, B.  
13 Winter, P. Jungwirth and S. E. Bradforth, *J. Am. Chem. Soc.*, 2015, **137**, 201-209.
- 14 86. Z. N. Heim and D. M. Neumark, *Acc. Chem. Res.*, 2022, **55**, 3652-3662.
- 15 87. S. Peng, A. Padva and P. R. LeBreton, *Proc. Natl. Acad. Sci. U.S.A.*, 1976, **73**, 2966-  
16 2968.
- 17 88. A. B. Trofimov, J. Schirmer, V. B. Kobychyev, A. W. Potts, D. M. P. Holland and L.  
18 Karlsson, *J. Phys. B*, 2005, **39**, 305-329.
- 19 89. C. Su, C. T. Middleton and B. Kohler, *J. Phys. Chem. B*, 2012, **116**, 10266-10274.
- 20 90. J. M. L. Pecourt, J. Peon and B. Kohler, *J. Am. Chem. Soc.*, 2001, **123**, 10370-10378.
- 21 91. M. K. Kuimova, J. Dyer, M. W. George, D. C. Grills, J. M. Kelly, P. Matousek, A. W.  
22 Parker, X. Z. Sun, M. Towrie and A. M. Whelan, *Chem. Commun.*, 2005, **9**, 1182-1184.
- 23 92. G. W. Doorley, M. Wojdyla, G. W. Watson, M. Towrie, A. W. Parker, J. M. Kelly and  
24 S. J. Quinn, *J. Phys. Chem. Lett.*, 2013, **4**, 2739-2744.
- 25 93. N. Ikeda, N. Nakashima and K. Yoshihara, *J. Phys. Chem.*, 1984, **88**, 5803-5806.

- 1 94. H. Miyasaka, M. Hagihara, T. Okada and N. Mataga, *Chem. Phys. Lett.*, 1992, **188**,  
2 259-264.
- 3 95. H. Xu and S. Pratt, *J. Phys. Chem. A*, 2013, **117**, 9331-9342.
- 4 96. N. J. Kim, G. Jeong, Y. S. Kim, J. Sung, S. Keun Kim and Y. D. Park, *J. Chem. Phys.*,  
5 2000, **113**, 10051-10055.
- 6 97. Y. Lee, M. Schmitt, K. Kleinermanns and B. Kim, *J. Phys. Chem. A*, 2006, **110**, 11819-  
7 11823.
- 8 98. C. Plützer and K. Kleinermanns, *Phys. Chem. Chem. Phys.*, 2002, **4**, 4877-4882.
- 9 99. A. Broo, *J. Phys. Chem. A*, 1998, **102**, 526-531.
- 10 100. R. W. Wilson and P. R. Callis, *Photochem. Photobiol.*, 1980, **31**, 323-327.
- 11 101. C. M. Marian, M. Kleinschmidt and J. Tatchen, *Chem. Phys.*, 2008, **347**, 346-359.
- 12 102. Y.-i. Yamamoto and T. Suzuki, *J. Phys. Chem. Lett.*, 2020, **11**, 5510-5516.

13

14